Received 19 October 2022; revised 27 November 2022; accepted 4 December 2022. Date of publication 9 December 2022;
date of current version 23 January 2023.

Digital Object Identifier 10.1109/OJAP.2022.3227903

Efficiency-Driven Design for Planar Antennas With Lossy Materials

PURNA B. SAMAL [1] (Graduate Student Member, IEEE), SHENGJIAN J. CHEN [1,2] (Member, IEEE), TRAN T. TUNG [3], DUSAN LOSIC [3], AND CHRISTOPHE FUMEAUX [1] (Fellow, IEEE)

[1]School of Electrical and Electronics Engineering, The University of Adelaide, Adelaide, SA 5005, Australia

[2]College of Science and Engineering, Flinders University, Adelaide, SA 5042, Australia

[3]ARC Graphene Research Hub, School of Chemical Engineering and Advanced Materials, The University of Adelaide, Adelaide, SA 5005, Australia

CORRESPONDING AUTHOR: P. B. SAMAL (e-mail: purna.samal@adelaide.edu.au)

This work was supported by the ARC Research Hub for Graphene Enabled Industry Transformation, funding under Industrial Transformation Research Hub, The University of Adelaide under Grant IH150100003.

ABSTRACT This article demonstrates a design strategy for improving the radiation efficiency of a planar antenna made of a layered conductor of MXene with modest conductivity on a lossy PDMS substrate. New methods to reduce the conductor loss and the dielectric loss are proposed. On the one hand, the conductor loss is minimized by identifying the location of high current density on the antenna radiator, and then accordingly altering its shape to redistribute the surface currents as uniformly as possible. On the other hand, the dielectric loss is reduced by employing a folded ground plane with elevated edges. This ground plane structure reduces the concentration of the electric field in the dielectric substrate and thus minimizes the power dissipation due to dielectric loss. The improvement techniques are implemented starting from a standard U-slot microstrip antenna. The method demonstrates to improve the radiation efficiency significantly by an average of 14% for a microstrip antenna fabricated using MXene conductor with a sheet resistance of 2 Ω/square and a lossy PDMS substrate. Importantly, the proposed method can preserve the overall antenna size and the operating frequency band. The optimized antenna exhibits a high radiation efficiency of 71% and offers a wide impedance bandwidth of 56% covering operation for the 5 GHz WLAN band.

INDEX TERMS Non-metallic antennas, flexible antennas, microstrip patch antennas, radiation efficiency, wideband, wireless body area network, wireless local area network.

I. INTRODUCTION

RADIATION efficiency, one of the key performance indicators of an antenna, is determined by the conductor loss and the dielectric loss. These losses are primarily influenced by choice of the conductor and the dielectric materials used in the antenna design. In wearable applications, flexible materials are preferred, as they offer comfort to the user with suitable mechanical properties. Recently, non-ideal conductors have received a lot of attention in wearable antenna design due to their attractive features: environmental friendliness, high corrosion-resistance, light weight, flexibility, wearability or low cost. Popular non-ideal conductors include carbon nanotube (CNT) composites [1], [2], [3], conductive polymers [4], [5], graphene [6], [7], [8] and MXene [9]. In parallel, other types of metal-based composite conductors have been increasingly explored to extract attractive features such as optical transparency for unobtrusive integration in windows, solar panels and displays. Most commonly used are indium tin oxide (ITO) [10], aluminium zinc oxide (AZO) [11], Ag-coated polyesters [12], AgHT-8 [13], conductive meshes [14] and graphene-based conductors [15]. Similarly, there are numerous flexible dielectric materials use for wearable applications. Few of the popular ones are the felt materials [16], PF4-foams [17], denim fabrics [18], polyethylene terephthalate (PET) [19] and polydimethylsiloxane (PDMS) [20], [21]. Similarly, some

dielectric materials, such as previously mentioned PDMS, can offer excellent mechanical and physical properties for wearable applications, however with a relatively high loss. Most of these unconventional conductive and dielectric materials are lossy leading to a relatively low antenna radiation efficiency and therefore, solutions to address this problem are of significant interest.

One of the major issues that limits the application of some of the mentioned non-ideal conductors is their low electrical conductivity [4], [22], [23], [24]. This results in low radiation efficiency which raises question on their suitability in many wearable applications. Transparent conductors exhibit similar behaviour, which leads generally to a trade-off between conductivity and transparency [25], [26], [27]. One of the conventional methods to increase the conductivity is to use a thicker layer of conductors [28]. However, thick conductors tend to become brittle and loose some of their flexibility and/or transparency. There are nevertheless various other methods proposed in the literature to improve the radiation efficiency of an antenna. For instance methods based on stacked conductors and multiple laminated thin conductors were presented in [29] and [30]. The latter demonstrated an efficiency improvement of 10.7%, however it requires a rather complex fabrication process and an additional optimization round to preserve the operating bandwidth. A method based on silver paste coating on the radiator areas with high current density was proposed in [31], while a similar concept using gold layer deposition in selected locations was demonstrated in [32] conjunction with transparent conductors. Although the proposed techniques demonstrated to improve the radiation efficiency and preserve the optical transparency, it required an extra localized deposition of material with a higher electrical conductivity. Similarly, some dielectric materials can offer excellent mechanical and physical properties for wearable applications, however with a relatively high loss. Therefore, to minimize the loss impact, several methods were proposed to reduce the dielectric loss. Partial removal of the dielectric materials is a common method to reduce the loss [33], [34], however with a reduced permittivity and increased fabrication complexity associated to substrates with heterogeneous materials.

In this work, we propose methods to reduce the ohmic loss and the dielectric loss of a flexible antenna made of non-ideal conductor and a lossy dielectric. The first proposed method minimizes the conductor loss by decreasing the maximum surface current density on the antenna conductor. This is achieved by selectively altering the shape of the radiator area where high current density are observed. The optimization of the radiating areas is based on two aspects: i) minimizing the concentration of high surface currents usually on the radiator edges [35], and ii) distributing the surface current on the radiator as uniformly as possible to achieve the maximum efficiency improvement [36]. Unlike the existing efficiency improvement methods, the proposed method maintains the overall antenna size, as it only alters the main radiator shape. Moreover, the method preserves the existing

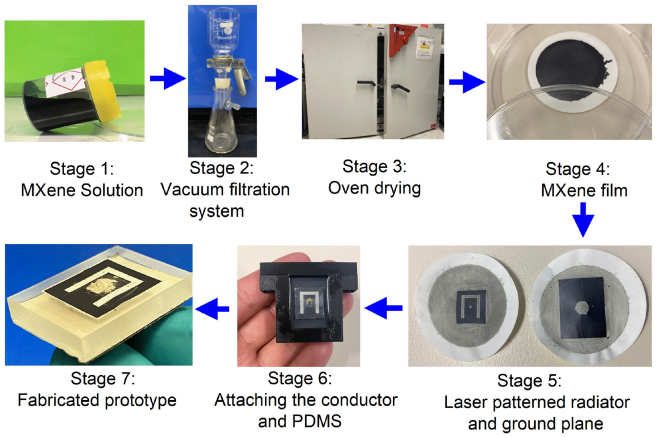

FIGURE 1. Schematic for preparation of MXene film conductor and antenna fabrication.

operational frequencies by maintaining the same resonant current length. The work also proposes a second method to improve the efficiency, by reducing the dielectric loss in patch-like geometries. The method extends the ground plane with folded elevated edges, which reduce the electric field density and thus lowers power dissipation in the dielectrics. Unlike the existing methods, the proposed method does not require physical modification of the dielectric substrate and offers a simple fabrication process.

To demonstrate the proposed methods, a moderately lossy MXene film is prepared with a predefined sheet resistance and used as an antenna conductor, and a lossy PDMS slab is used as the flexible substrate. The preparation of antenna materials and the fabrication process are presented in the next section. The implementation of the proposed methods is presented in Section III and Section IV describes the final results and experimental validation.

II. ANTENNA MATERIALS AND INITIAL DESIGN

MXene, a synthesis of titanium carbide ($Ti_3C_2T_x$) [37] is prepared as a conducting film from a MXene aqueous dispersion. Initially the dispersion is prepared by adding deionised water to the prepared MXene hydrogel. The mixture is then sonicated for an hour before the filtration process. About 4 ml of MXene dispersion is used to prepare a single MXene conductor film with thickness of 20 μm and a predefined sheet resistance of 2 Ω/square. The process of a film conductor preparation and the antenna fabrication process is briefly outlined in Fig. 1. Firstly, the prepared MXene dispersion is slowly filtered using a vacuum filtration system to form a conductive MXene film on a filter membrane. The hydrophilic filter membrane is a MF-Millipore with 0.22 μm pore size and diameter of 47 mm. The whole filtration setup is placed to dry in a vacuum drying oven for three hours at 60° C. The obtained film with a diameter of 32 mm is shown in Stage 4 of Fig. 1. The procedure is repeated to produce four MXene conductor films with similar sheet resistance and thickness. A pair of films are used to fabricate a single

antenna, i.e., one film for the antenna radiator and one for the ground plane. Generally, the MXene solution is uniformly deposited on the filter membrane. However, a consistent procedure for the material preparation is followed to maintain such a uniform deposition for a repeatable fabrication process. The procedure includes maintaining the same solution level of the MXene dispersion, the fixed duration for the filtration process, and the fixed duration for oven drying at a constant temperature. The desired antenna conductor shape (resonant patch or ground plane) is patterned from the films using a laser milling machine and a scalpel to remove excess material. An example of the patterned antenna conductor and ground plane are shown in Stage 5 of Fig. 1. Next, a single layer of sticky tape is applied over the top of the MXene conductor to prevent mechanical damage. The thickness of the sticky tape is 45 μm and it is considered during the antenna design process. The application of the sticky tape does not significantly affect the antenna performance, as confirmed through simulation. The relative permittivity $\varepsilon_r = 3$ and loss tangent tan $\delta = 0.01$, taken from [38] for similar sticky tape, are used for the simulation. The Stage 6 of the fabrication process involves attaching the conductor film on the PDMS substrate which has a relative permittivity ε_r of 2.7 and a loss tangent tan $\delta = 0.022$ at 6 GHz. A thin layer of polyvinyl acetate (PVA) glue is used to attach the conductor film to the PDMS substrate. The feed connectors are connected in the last stage using electrically conductive epoxy adhesive.

A microstrip antenna topology with an inverted U-slot radiator [39], [40], [41] is chosen as an initial antenna structure to demonstrate the implementation of the proposed efficiency improvement methods. All the simulations are performed using the time-domain solver in CST Studio Suite 2021 (CST). Initially, a rectangular microstrip antenna is designed to operate at 5.8 GHz. The operating frequency is mainly controlled by the patch length. Next, an inverted U-slot is introduced to obtain an additional resonance which is used to improve the operational bandwidth through resonance overlapping. The second resonance frequency is dominantly controlled by the slot length *ls* as indicated in Fig. 2 (a). A longer *ls* leads to a lower resonance frequency and *ws* can be used for tunning. The antenna is designed to operate at the 5 GHz band of wireless local area network (WLAN). A full ground plane is employed to reduce the back radiation [16]. The antenna is fed using a coaxial probe feed from the rear of the ground plane. The dimension details of the designed reference inverted U-slot microstrip antenna are shown in Fig. 2 (a). The gray shade in the figure is the antenna conductor MXene, while the white shade with black border line represents the PDMS substrate. The overall size of the inverted U-slot microstrip antenna is $0.36\lambda_0 \times 0.27\lambda_0 \times 0.06\lambda_0$ including the ground plane, where λ_0 is the free-space wavelength at the lowest operating frequency of 4.5 GHz. The corresponding fabricated prototype is presented in Fig. 2 (b). The simulated and the measured results of the reflection coefficient in free space

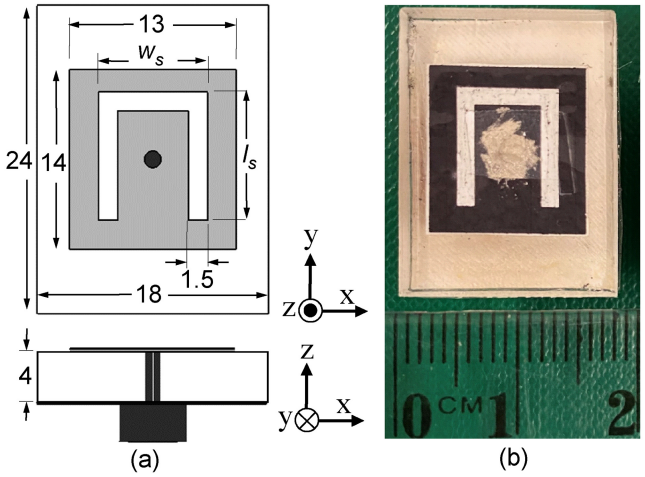

FIGURE 2. The structure of the initial reference design of inverted U-slot microstrip antenna with dimensions marked in mm: (a) simulation model and (b) fabricated prototype. The optimized values of the design parameter *ws* and *ls* are 8.5 mm and 10 mm respectively.

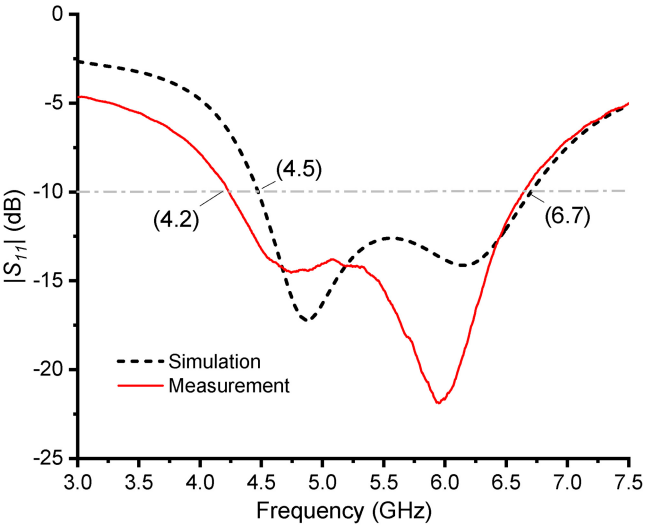

FIGURE 3. Simulated and measured reflection coefficient for the reference inverted U-slot microstrip antenna made of MXene conductor on a PDMS substrate.

are shown in Fig. 3. A reasonable agreement is observed between the simulation and measurement, with a 300 MHz bandwidth extension at the lower frequency end. The antenna prototype offers a wide impedance bandwidth of 45.9% operating from 4.2 to 6.7 GHz, which generously covers the targeted WLAN band. The simulated and the estimated radiation efficiencies are shown in Fig. 4. The radiation efficiency is estimated using the method of gain-directivity comparison as applied in [42], [43]. The efficiency is evaluated within the operating band from 4.7 to 6.3 GHz, with an average value of 57%. The low efficiency is expected due to relatively high sheet resistance of the conductor of 2 Ω/square, and the lossy PDMS substrate with a loss tangent of 0.022.

This motivates us to improve the radiation efficiency of the antenna using various techniques as presented in the following section.

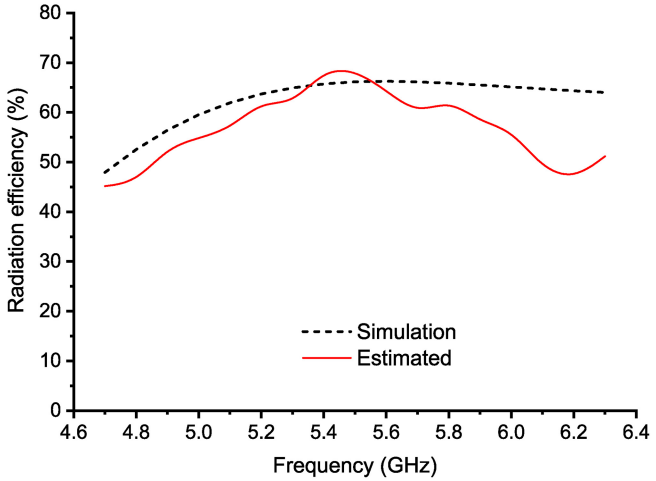

FIGURE 4. Simulated and estimated radiation efficiency of the reference inverted U-slot microstrip antenna made of MXene conductor on a PDMS substrate.

III. EFFICIENCY IMPROVEMENT

The MXene conductor loss and the PDMS dielectric loss predominantly determine the radiation efficiency of the antenna. Therefore, these losses are separately evaluated through simulations within the operating band from 4.7 to 6.3 GHz. The simulated conductor and dielectric losses of the reference U-slot microstrip antenna are presented as a red solid line in Fig. 5 (b) and (c), respectively. For clarity, the simulated reflection coefficient and radiation efficiency are also presented in Fig. 5 (a) and (d), respectively. As can be seen from Fig. 5 (b), the antenna suffers an average conductor loss corresponding to around 25% of its accepted power. Similarly, the PDMS substrate causes an average dielectric loss of 11% of the accepted power. The losses appear higher at lower frequencies which translates in lower radiation efficiency as observed in Fig. 5 (d). To identify the regions of the radiator area that dominantly contribute to the conductor loss, the maximum surface current distribution is evaluated. The evaluated results at 5 and 6 GHz are shown in Fig. 6 (a) for an input power of 0.5 W. These two frequency points are chosen as they are representative of the general distribution patterns of surface current throughout the operating bandwidth. The antenna shows a maximum surface current density of 99.7 A/m at 5 GHz and 140.2 A/m at 6 GHz. At 5 GHz, a high current density is observed along the outer edges of the radiator length. Similarly, higher density of surface current appears along the edges of the inverted U-slot at both 5 and 6 GHz. As these radiator areas with high surface current density dominantly contribute to the ohmic loss, the efficiency improvement method is primarily targeting these areas. The method alters theses areas with an objective to progressively reduce the maximum surface current density over the conductor area, thus progressively equalizing the current density distribution over the surface. The reduction enables to decrease the ohmic loss and therefore improve the antenna radiation efficiency.

A. CIRCULAR RADIATOR

To portray the evolution sequence of radiator shape and size, the initial inverted U-slot topology is included as shown in Fig. 7 (a). Importantly, while changing the radiator shape and size, the overall antenna size is kept constant, that is, the substrate and ground plane sizes remain the same along with their thickness. The resonant current length also needs to be maintained to preserve the operating frequency band. The first efficiency improvement method is applied to reduce the maximum surface current density along the outer edge of the radiator length. This is achieved by replacing the rectangular radiator with a circular radiator as shown in Fig. 7 (b). Beside offering a wider area for current flow along the radiator length, the circular radiator eliminates the sharp corners of the rectangular shape. This enables to reduce the maximum surface current density as shown by the current distribution presented in Fig. 6 (b). Compared to the rectangular radiator, the circular radiator decreases the maximum surface current density from 99.7 to 93.6 A/m at 5 GHz. Similarly at 6 GHz, the maximum current value is reduced to 127.1 from the initial of 140.2 A/m. A similar observation that the circular patch shape offers a higher radiation efficiency than a rectangular counterpart was reported in [44]. The simulated reflection coefficient corresponding to the circular radiator is shown in Fig. 5 (a), indicated by the red dash curve. The operational bandwidth is well maintained.

The circular radiator reduces the conductor loss and dielectric loss by an average value of 4% and 0.8% respectively. The corresponding losses are shown in Fig. 5 (b) and (c), indicated by red dash curve. This results in a marked improvement of the radiation efficiency as shown in Fig. 5 (d).

B. HORSE-SHOE SLOT MICROSTRIP RADIATOR

In the second stage, the radiation efficiency is further improved by reducing the maximum current density along the edges of the inverted U-slot. To achieve this, the sharp straight edges of the inverted rectangular U-slot are eliminated by introducing a smoothly curved inverted U-slot as shown in Fig. 7 (c). The sharp corners at the slot extremities are also modified through rounding, leading to a smoother ending. While employing these modifications, the resonant current length along the slot is maintained to preserve the operating frequencies. Next, the maximum surface current density is further reduced by optimizing the slot width and increasing its area along the length of the radiator. The radiator area between the edge of the radiator and the edge of a slot leg still indicates high density of surface currents. As this area contributes significantly towards the effective resistance offered by the radiator, this particular area is widened to reduce the effective resistance. Moreover, the widened areas allow uniform spread of the surface current [36] thereby reducing the maximal current density. This addition results into a modified circular radiator with smooth inverted U-slot as shown in Fig. 7 (c). As the slot structure looks like a horse

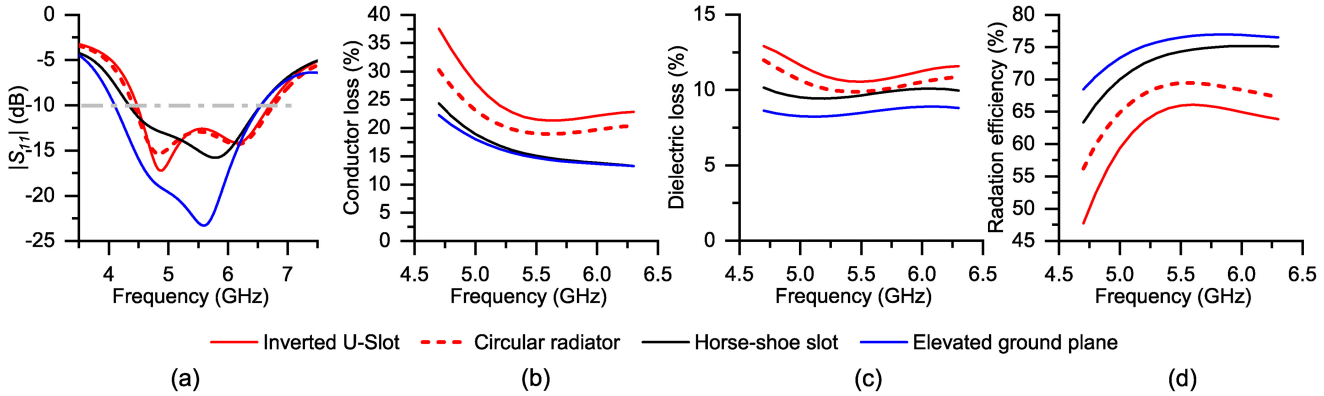

FIGURE 5. The simulated results of (a) reflection coefficient (b) conductor loss (c) dielectric loss (d) radiation efficiency.

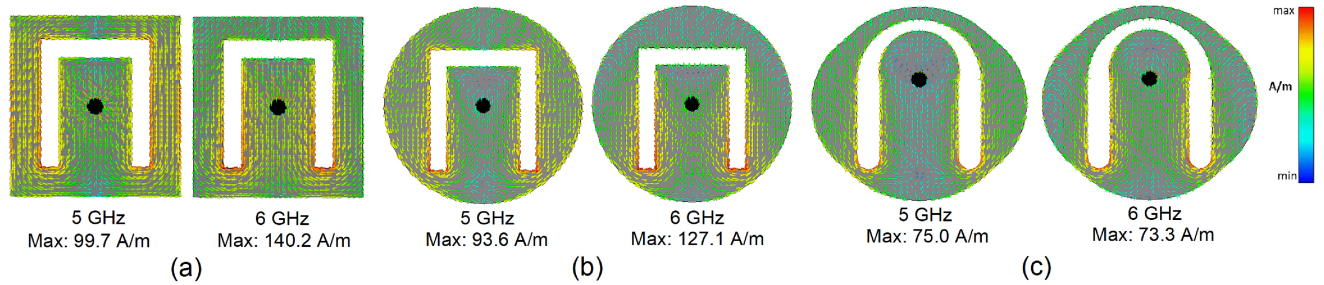

FIGURE 6. The simulated surface current distribution of (a) the original inverted U-slot microstrip antenna (b) the circular radiator and (c) the radiator of horse-shoe slot microstrip antenna.

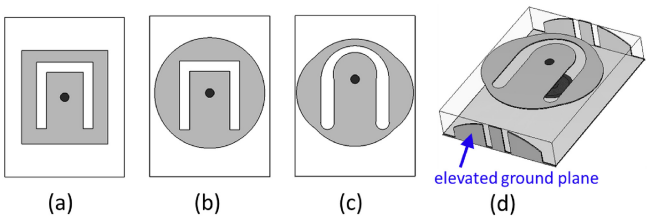

FIGURE 7. The evolution of radiator and slot shape with decreasing maximum surface current density (a) inverted U-slot microstrip antenna (b) circular radiator (d) horse-shoe slot microstrip antenna and (d) horse-shoe slot microstrip antenna with elevated ground plane.

shoe, the antenna is referred as a horse-shoe slot microstrip antenna.

The simulated reflection coefficient of the horse-shoe slot microstrip antenna is shown in Fig. 5 (a), indicated by a solid black curve. The operation bandwidth is well maintained. The applied modification further decreases the maximum surface current density by 19.9% and 42.6% at 5 and 6 GHz and improves the radiation efficiency by 6%. The surface current distributions are shown in Fig. 6 (c). The losses are further reduced by 4.95% and 0.7% are shown in Fig. 5 (b) and (c), indicated by straight black curve, noting that this technique predominantly improves conduction efficiency. The corresponding radiation efficiency, indicated by a solid black curve is shown in Fig. 5 (d). The horse-shoe slot antenna achieves an average radiation efficiency of 73% within the operating bandwidth.

C. ELEVATED GROUND PLANE

In the third stage, the ground plane shape is modified to reduce the dielectric loss and thus further improve the radiation efficiency. The ground plane is extended at the two ends by folding and elevating the edges along the substrate as shown in Fig. 7 (d). The elevated ground plane extends from the ground plane to the top layer and its shape is optimized with a curve ending to reduce the dielectric loss. Moreover four vertical slits are introduced at the edges and the center of the elevated ground plane to relax the mechanical stress while bending. The optimized antenna structure is referred as horse-shoe slot microstrip antenna with elevated ground plane.

The optimized structure of the elevated ground plane can further reduce the dielectric loss as shown in Fig. 5 (c) indicated by the blue curve. In terms of physical interpretation, the structure minimizes the concentration of electromagnetic energy density trapped within the dielectric material and thus lowers the dielectric loss by an average value of 2.1% within the operating bandwidth. Moreover, the method of elevating the ground plane is generally expected to be also applicable to different substrate lengths. As the dielectric loss corresponds to the power loss due to dielectric heating, the power loss density in the substrate is further evaluated at 5 and 6 GHz for better physical insight. The simulation results with a cut-plane in the z-axis at $z = 3$ mm (i.e., within the substrate height) are compared in Fig. 8. Specifically, Fig. 8 (a) shows the power loss density of the horse-shoe

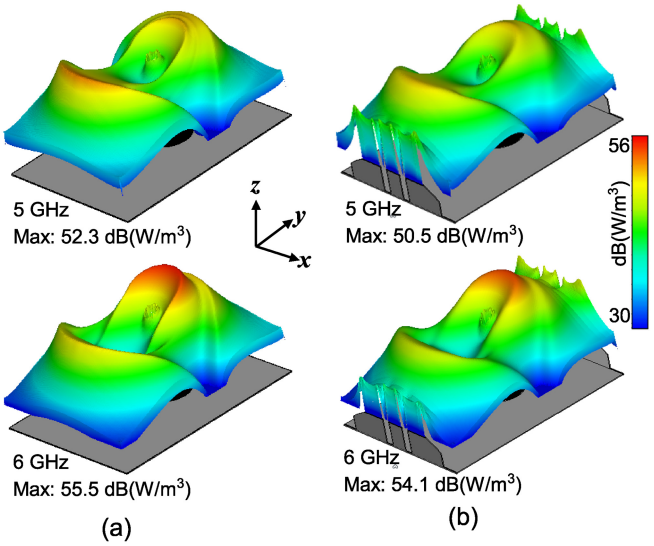

FIGURE 8. The simulated power loss density at cut-plane z = 3 mm for (a) the horse-shoe slot microstrip antenna and (b) the horse-shoe slot microstrip antenna with elevated ground plane.

slot microstrip antenna, whereas the power loss density with elevated ground plane are shown in Fig. 8 (b). As seen from the figure, the elevated structure reduces the maximum power loss density by 1.8 dB and 1.4 dB at 5 and 6 GHz respectively. The reduction in dielectric loss further improves the radiation efficiency by 2.5% as shown in Fig. 5 (d). A negligible effect on the conductor loss is observed. The corresponding simulated reflection coefficient is shown in Fig. 5 (a). It is also noted that the proposed elevated ground plane not only preserves the operational bandwidth, it further extends it by 250 MHz towards lower frequencies.

IV. FINAL RESULTS

The dimension details of the horse-shoe slot microstrip antenna with elevated ground plane are shown in Fig. 9 (a). The overall antenna size remains the same as that of the reference inverted U-slot microstrip antenna, i.e., $24 \times 18 \times 4.2$ mm^3. The fabricated prototype is presented in Fig. 9 (b) and (c).

A. IMPEDANCE BANDWIDTH

The simulated and the measured reflection coefficients are presented in Fig. 10 for the final design. The proposed antenna offers a wide impedance bandwidth of 56% operating from 3.5 to 6.6 GHz in free space. The measurement agrees well with the simulation. A shift in operating band by 600 MHz towards the lower frequencies in the measured reflection coefficient is observed, which is possibly due to the blunt vertical folding of the elevated ground plane, see Fig. 9 (c). This is in contrast to the simulation environment, where the elevated ground plane is folded vertically by a sharp 90° bend.

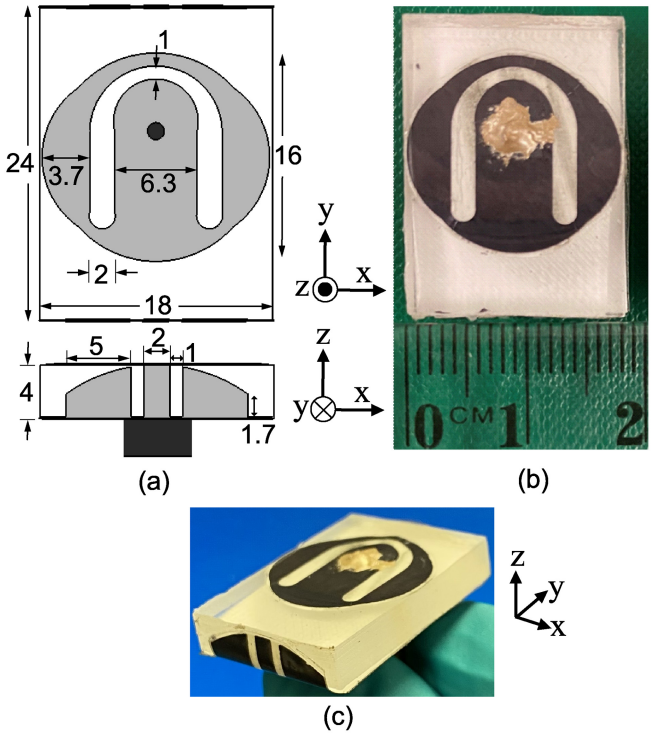

FIGURE 9. The structure of horse-shoe slot microstrip antenna with elevated ground plane with dimensions marked in mm: (a) simulation model, (b) top view and (c) the perspective view of the fabricated prototype.

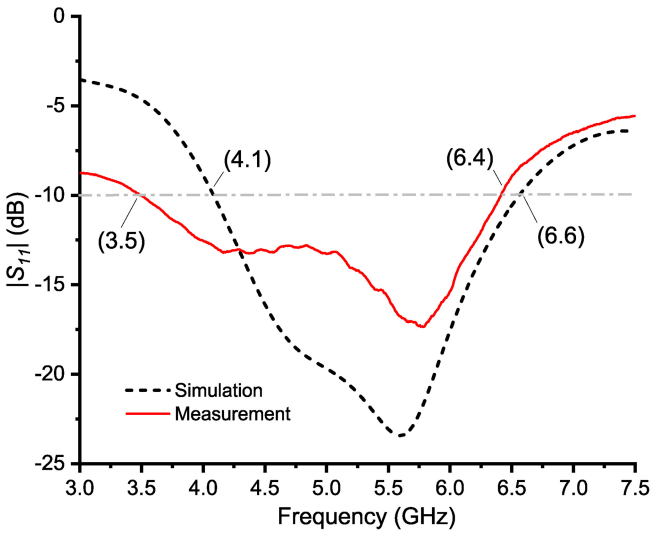

FIGURE 10. Simulated and measured reflection coefficient of the final design of the horse-shoe slot microstrip antenna.

B. RADIATION PATTERN AND GAIN

The measurement of the radiation patterns for the final design is performed in an anechoic chamber. The evaluated free-space normalized gain patterns at 5 and 6 GHz are shown in Fig. 11 (a) and (b) respectively. A good agreement between the simulated and the experimental patterns is achieved for both *xz*-(E-) and *yz*-(H-) plane. The

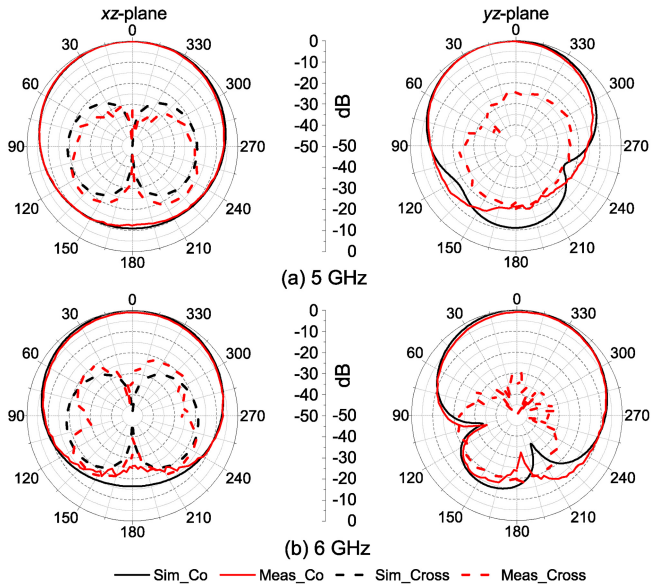

FIGURE 11. Free-space normalized radiation patterns of the final design in the *xz*-plane and *yz*- plane at (a) 5 GHz and (b) 6 GHz.

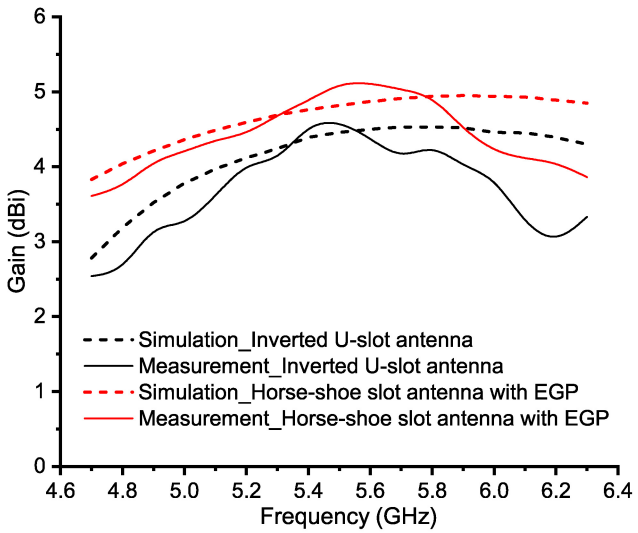

FIGURE 12. Simulated and measured maximum gain of the inverted U-slot microstrip antenna and the horse-shoe slot microstrip antenna with elevated ground plane (EGP).

proposed antenna exhibits directional radiation pattern with a broadside maximum in both planes.

The simulated and measured maximum gain for free-space operation is shown in Fig. 12. The figure depicts an acceptable agreement between the simulation and the measurement. The proposed antenna offers an average gain of 4.4 dBi when evaluated from 4.7 to 6.3 GHz. For comparison, the simulated and the measured gain of the initial inverted U-slot microstrip antenna (reference) are also shown in Fig. 12. The curves indicate an acceptable agreement between the simulated and the measured gain. In general, the applied efficiency improvement methods demonstrate to

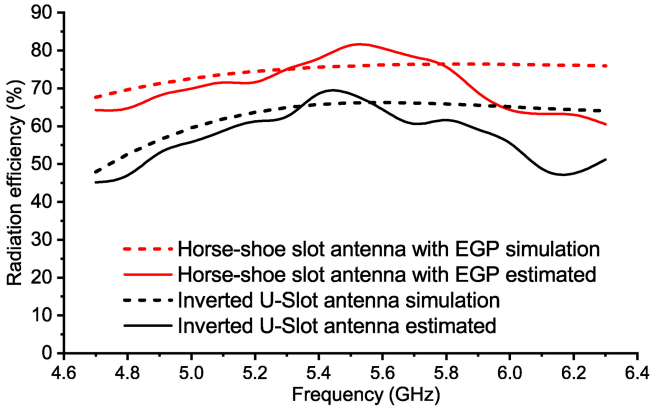

FIGURE 13. Simulated and estimated radiation efficiency of the horse-shoe slot microstrip antenna with elevated ground plane (EGP), with comparison to the reference antenna.

slightly increase the maximum free-space gain by an average value of 0.72 dBi, within the operating band.

C. RADIATION EFFICIENCY

The simulated and the estimated radiation efficiencies of the horse-shoe slot microstrip antenna with elevated ground plane are shown in Fig. 13, where a good agreement is observed. Compared to the initial inverted U-slot microstrip antenna (reference), the proposed efficiency improvement method increases the radiation efficiency by an average value of 14%. The estimated radiation efficiency of the inverted U-slot antenna is indicated by black solid curve in Fig. 13. The resulting proposed antenna achieves an average radiation efficiency of 71% when computed within the operating band from 4.7 to 6.3 GHz.

To further illustrate the improvement, thermal images are captured to visualize the conductor loss in the form of heat using a FLIR E53 Advanced Thermal Imaging Camera. The camera offers a wide temperature reading range from −20 to 120°C. The measurement setup consist of a signal generator and an RF power amplifier as presented in [45]. An EXG analog signal generator N5173B by Keysight with operating frequency range from 9 kHz to 20 GHz is used to generate a continuous waveform (CW) sinusoidal reference signal at 4.7 GHz. Prior to feeding the signal to an antenna, a ZHL-42 RF amplifier is used to amplify the signal to attain a signal power of 20.8 dBm. The measurements are performed in an anechoic chamber. The room lights were turned off and black absorbers covered the connectors to minimize the thermal noise caused by the reflecting objects. The thermal images are recorded before and after antenna excitation with a fixed input power of 120 mW at the lower operating band of 4.7 GHz. The captured thermal images of the reference inverted U-slot antenna before and after the excitation are shown in Fig. 14 (a) and (b) respectively. For reference, the corresponding simulated surface current distribution on the radiator at 4.7 GHz is shown in Fig. 14 (c). Similarly, the captured thermal images of the optimized horse-shoe slot antenna with elevated ground plane and the surface current distribution are presented in

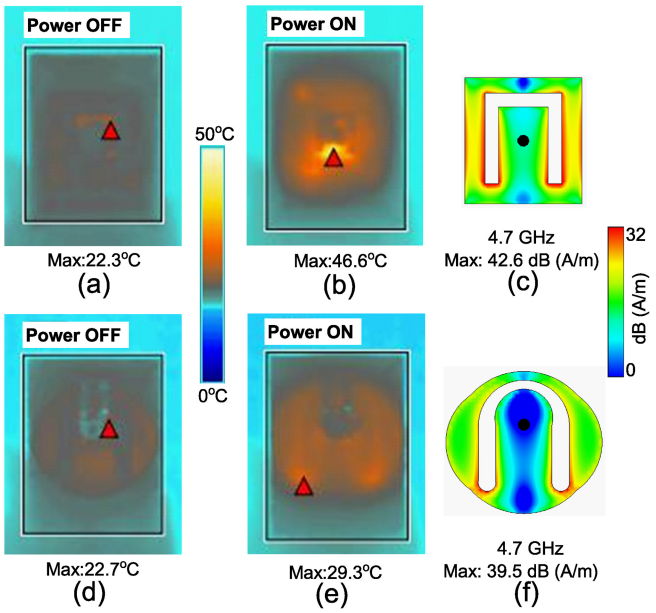

FIGURE 14. Top row: Captured thermal images of the reference inverted U-slot microstrip antenna (a) before excitation, (b) after excitation and (c) simulated surface current distribution on the radiator. Bottom row: Captured thermal images of the optimized horse-shoe slot microstrip antenna with elevated ground plane (d) before excitation, (e) after excitation and (f) simulated surface current distribution. The small red triangular indicator in the figures represents the hottest point with the maximum temperature indicated below each sub-figure.

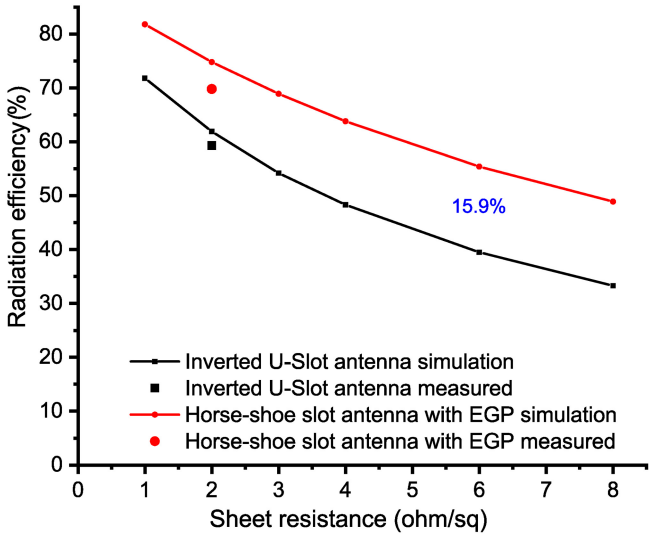

FIGURE 15. Simulated prediction of improvement in radiation efficiency through the proposed method.

Fig. 14 (d), (e) and (f) respectively. In case of the reference U-slot microstrip antenna, the excitation increases the maximum temperature on the radiator from 22.3°C to 46.6°C. The hottest location is indicated by a small red triangle in the figures. The higher value of the temperature and the non-uniform heat distribution indicates a higher conductor loss thereby a reduced radiation efficiency. The heat distribution generally agrees with the surface current distribution shown in Fig. 14 (c), with our interpretation being that the two hot spots of the inner slots are likely merging in the antenna centre due to heat conduction. On the contrary, the horse-shoe slot microstrip antenna with elevated ground plane offers a significantly lower rise in the maximum temperature from 22.7°C to 29.3°C. Moreover, the optimized structure distributes the heat more uniformly which is indicative of a more uniform current distribution. The location of the hottest spot agrees well with the simulation, which is at the edges of the inverted U-slot. The thermal measurement further demonstrates that the proposed method minimizes the concentration of high surface currents and uniformly distributes the surface current density on the radiator, thereby reducing the ohmic loss.

Finally, to predict the efficiency improvement offered by the proposed methods, the initial inverted U-slot microstrip antenna and the optimized horse-shoe slot microstrip antenna with elevated ground plane are simulated with different values of conductor sheet resistance. The relationship between the sheet resistance and the simulated radiation efficiency are shown in Fig. 15. The simulated results indicate that the proposed efficiency improvement method exhibits an increasing effectiveness in efficiency improvement with a higher sheet resistance. As predicted through simulations for conductors with a high sheet resistance of 6 Ω/square, the improvement in radiation efficiency of 15.9% can be achieved. This further highlights the potential application of the proposed efficiency improvement methods not only for non-ideal flexible antennas (as presented here), but also for non-metallic and transparent antennas with high sheet resistance.

V. CONCLUSION

Methods to improve the radiation efficiency of an antenna with a designed relatively high sheet resistance and lossy dielectrics have been presented. The proposed methods have been demonstrated on an inverted U-slot microstrip antenna. The antenna has been designed using an advanced 2D $Ti_3C_2T_x$ MXene conductor on a lossy PDMS substrate. For illustration, the MXene film has been produced with a sheet resistance of 2 Ω/square for a 20 μm thickness, deposited on a filter membrane. The work demonstrates a total radiation efficiency improvement of 14%, which leads to a final average radiation efficiency of 71%. The principle of the improvement technique is based on two aspects. First, it alters the radiator shape to reduce the maximum surface current density, which in turn decreases the conductor ohmic loss. Secondly, it alters the ground plane shape by raising its edges to minimize the dielectric loss. The structure exhibits a decreased concentration of electromagnetic energy density trapped within the dielectric material thereby reducing the losses due to the dielectric heating. The proposed technique maintains the existing overall antenna size and preserves the operating bandwidth. It also exhibits a potential to improve the efficiency of antennas based on other unconventional lossy conductors. For instance, one can apply similar

techniques to improve efficiency for optically transparent antennas while preserving their transparency.

ACKNOWLEDGMENT

The authors would like to thank Alban O'Brien from The University of Adelaide for his assistance with the antenna fabrication.

REFERENCES

[1] A. Mehdipour, I. D. Rosca, A. Sebak, C. W. Trueman, and S. V. Hoa, "Full-composite fractal antenna using carbon nanotubes for multiband wireless applications," *IEEE Antennas Wireless Propag. Lett.*, vol. 9, pp. 891–894, 2010.

[2] A. Mehdipour, T. A. Denidni, A. Sebak, C. W. Trueman, I. D. Rosca, and S. V. Hoa, "Nonmetallic dielectric resonator antenna using carbon nanotube composite materials," *IEEE Antennas Wireless Propag. Lett.*, vol. 11, pp. 1293–1295, 2012.

[3] Z. Hamouda, J.-L. Wojkiewicz, A. A. Pud, L. Koné, S. Bergheul, and T. Lasri, "Magnetodielectric nanocomposite polymer-based dual-band flexible antenna for wearable applications," *IEEE Trans. Antennas Propag.*, vol. 66, no. 7, pp. 3271–3277, Jul. 2018.

[4] H. Rmili, J.-L. Miane, H. Zangar, and T. Olinga, "Design of microstrip-fed proximity-coupled conducting polymer patch antenna," *Microw. Opt. Technol. Lett.*, vol. 48, no. 4, pp. 655–660, 2006.

[5] A. Verma, C. Fumeaux, V.-T. Truong, and B. D. Bates, "A 2 GHz polypyrrole microstrip patch antenna on Plexiglas-substrate," in *Proc. Asia Pacific Microw. Conf.*, 2009, pp. 36–39.

[6] J. Perruisseau-Carrier, "Graphene for antenna applications: Opportunities and challenges from microwaves to THz," in *Proc. Loughborough Antennas Propag. Conf. (LAPC)*, 2012, pp. 1–4.

[7] S. J. Chen, C. Fumeaux, T. T. Tung, and D. Losic, "High-efficiency microwave graphene antenna," in *Proc. IEEE Int. Symp. Antennas Propag. USNC/URSI Nat. Radio Sci. Meeting*, 2017, pp. 317–318.

[8] P. Kopyt et al., "Graphene-based dipole antenna for a UHF RFID tag," *IEEE Trans. Antennas Propag.*, vol. 64, no. 7, pp. 2862–2868, Jul. 2016.

[9] B. Sindhu, V. Adepu, P. Sahatiya, and S. Nandi, "An MXene based flexible patch antenna for pressure and level sensing applications," *FlatChem*, vol. 33, May 2022, Art. no. 100367.

[10] Y. Yao, W. Chen, X. Chen, and J. Yu, "Design of optically transparent antenna with directional radiation patterns," *Int. J. Antennas Propag.*, vol. 2017, Aug. 2017, Art. no. 8125432.

[11] M. E. Zamudio, T. Busani, Y. Tawk, J. Costantine, and C. Christodoulou, "Design of AZO film for optically transparent antennas," in *Proc. IEEE Int. Symp. Antennas Propag. (APSURSI)*, 2016, pp. 127–128.

[12] M. A. Malek, S. Hakimi, S. K. A. Rahim, and A. K. Evizal, "Dual-band CPW-fed transparent antenna for active RFID tags," *IEEE Antennas Wireless Propag. Lett.*, vol. 14, pp. 919–922, 2015.

[13] S. Hakimi, S. K. A. Rahim, M. Abedian, S. M. Noghabaei, and M. Khalily, "CPW-fed transparent antenna for extended ultrawideband applications," *IEEE Antennas Wireless Propag. Lett.*, vol. 13, pp. 1251–1254, 2014.

[14] S. H. Kang and C. W. Jung, "Transparent patch antenna using metal mesh," *IEEE Trans. Antennas Propag.*, vol. 66, no. 4, pp. 2095–2100, Apr. 2018.

[15] M. Grande et al., "Optically transparent wideband CVD graphene-based microwave antennas," *Appl. Phys. Lett.*, vol. 112, no. 25, 2018, Art. no. 251103.

[16] P. B. Samal, P. J. Soh, and G. A. E. Vandenbosch, "UWB all-textile antenna with full ground plane for off-body WBAN communications," *IEEE Trans. Antennas Propag.*, vol. 62, no. 1, pp. 102–108, Jan. 2014.

[17] S. J. Chen, T. Kaufmann, D. C. Ranasinghe, and C. Fumeaux, "A modular textile antenna design using snap-on buttons for wearable applications," *IEEE Trans. Antennas Propag.*, vol. 64, no. 3, pp. 894–903, Mar. 2016.

[18] S. Velan et al., "Dual-band EBG integrated monopole antenna deploying fractal geometry for wearable applications," *IEEE Antennas Wireless Propag. Lett.*, vol. 14, pp. 249–252, 2015.

[19] G. A. Casula, G. Montisci, and G. Mazzarella, "A wideband PET inkjet-printed antenna for UHF RFID," *IEEE Antennas Wireless Propag. Lett.*, vol. 12, pp. 1400–1403, 2013.

[20] R. B. V. B. Simorangkir, A. Kiourti, and K. P. Esselle, "UWB wearable antenna with a full ground plane based on PDMS-embedded conductive fabric," *IEEE Antennas Wireless Propag. Lett.*, vol. 17, no. 3, pp. 493–496, Mar. 2018.

[21] P. B. Samal, S. J. Chen, Q. Zhang, and C. Fumeaux, "A PDMS-based low-profile monopole antenna for wearable applications," in *Proc. IEEE MTT-S Int. Microw. Biomed. Conf. (IMBioC)*, 2022, pp. 271–273.

[22] M. Akbari, M. W. A. Khan, M. Hasani, T. Björninen, L. Sydänheimo, and L. Ukkonen, "Fabrication and characterization of graphene antenna for low-cost and environmentally friendly RFID tags," *IEEE Antennas Wireless Propag. Lett.*, vol. 15, pp. 1569–1572, 2016.

[23] T. Leng, X. Huang, K. Chang, J. Chen, M. A. Abdalla, and Z. Hu, "Graphene nanoflakes printed flexible meandered-line dipole antenna on paper substrate for low-cost RFID and sensing applications," *IEEE Antennas Wireless Propag. Lett.*, vol. 15, pp. 1565–1568, 2016.

[24] A. Mehdipour, I. D. Rosca, A. Sebak, C. W. Trueman, and S. V. Hoa, "Carbon nanotube composites for wideband millimeter-wave antenna applications," *IEEE Trans. Antennas Propag.*, vol. 59, no. 10, pp. 3572–3578, Oct. 2011.

[25] G. Haacke, "New figure of merit for transparent conductors,"*J. Appl. Phys.*, vol. 47, no. 9, pp. 4086–4089, 1976.

[26] Z. J. Silva, C. R. Valenta, and G. D. Durgin, "Optically transparent antennas: A survey of transparent microwave conductor performance and applications," *IEEE Antennas Propag. Mag.*, vol. 63, no. 1, pp. 27–39, Feb. 2021.

[27] A. S. M. Sayem, R. B. V. B. Simorangkir, K. P. Esselle, and R. M. Hashmi, "Development of robust transparent conformal antennas based on conductive mesh-polymer composite for unobtrusive wearable applications," *IEEE Trans. Antennas Propag.*, vol. 67, no. 12, pp. 7216–7224, Dec. 2019.

[28] A. S. M. Sayem, A. Lalbakhsh, K. P. Esselle, J. L. Buckley, B. O'Flynn, and R. B. V. B. Simorangkir, "Flexible transparent antennas: Advancements, challenges, and prospects," *IEEE Open J. Antennas Propag.*, vol. 3, pp. 1109–1133, Sep. 2022.

[29] H. Maema and T. Fukusako, "Radiation efficiency improvement for electrically small and low-profile antenna by stacked elements," *IEEE Antennas Wireless Propag. Lett.*, vol. 13, pp. 305–308, 2014.

[30] S. I. Latif, L. Shafai, and C. Shafai, "An engineered conductor for gain and efficiency improvement of miniaturized microstrip antennas," *IEEE Antennas Propag. Mag.*, vol. 55, no. 2, pp. 77–90, Apr. 2013.

[31] H. J. Song, T. Y. Hsu, D. F. Sievenpiper, H. P. Hsu, J. Schaffner, and E. Yasan, "A method for improving the efficiency of transparent film antennas," *IEEE Antennas Wireless Propag. Lett.*, vol. 7, pp. 753–756, 2008.

[32] M. R. Haraty, M. Naser-Moghadasi, A. A. Lotfi-Neyestanak, and A. Nikfarjam, "Improving the efficiency of transparent antenna using gold nanolayer deposition," *IEEE Antennas Wireless Propag. Lett.*, vol. 15, pp. 4–7, 2016.

[33] G. P. Gauthier, A. Courtay, and G. M. Rebeiz, "Microstrip antennas on synthesized low dielectric-constant substrates," *IEEE Trans. Antennas Propag.*, vol. 45, no. 8, pp. 1310–1314, Aug. 1997.

[34] S. B. Yeap and Z. N. Chen, "Microstrip patch antennas with enhanced gain by partial substrate removal," *IEEE Trans. Antennas Propag.*, vol. 58, no. 9, pp. 2811–2816, Sep. 2010.

[35] J. Oh and K. Sarabandi, "A topology-based miniaturization of circularly polarized patch antennas," *IEEE Trans. Antennas Propag.*, vol. 61, no. 3, pp. 1422–1426, Mar. 2013.

[36] M. Shahpari and D. V. Thiel, "Fundamental limitations for antenna radiation efficiency," *IEEE Trans. Antennas Propag.*, vol. 66, no. 8, pp. 3894–3901, Aug. 2018.

[37] M. Alhabeb et al., "Guidelines for synthesis and processing of two-dimensional titanium carbide (Ti3C2Tx MXene)," *Chem. Mater.*, vol. 29, no. 18, pp. 7633–7644, 2017.

[38] S. J. Chen et al., "A compact, highly efficient and flexible polymer ultra-wideband antenna," *IEEE Antennas Wireless Propag. Lett.*, vol. 14, pp. 1207–1210, 2015.

[39] A. Khidre, K. Lee, A. Z. Elsherbeni, and F. Yang, "Wide band dual-beam U-slot microstrip antenna,"*IEEE Trans. Antennas Propag.*, vol. 61, no. 3, pp. 1415–1418, Mar. 2013.

[40] K. F. Lee, S. S. Yang, A. Kishk, and K. M. Luk, "The versatile U-slot patch antenna,"*IEEE Antennas Propag. Mag.*, vol. 52, no. 1, pp. 71–88, Feb. 2010.

[41] T. Huynh and K. F. Lee, "Single-layer single-patch wideband microstrip antenna," *Electron. Lett.*, vol. 31, no. 16, pp. 1310–1312, Aug. 1995.
[42] T. Kaufmann, A. Verma, V.-T. Truong, B. Weng, R. Shepherd, and C. Fumeaux, "Efficiency of a compact elliptical planar ultra-wideband antenna based on conductive polymers," *Int. J. Antennas Propag.*, vol. 2012, Apr. 2012, Art. no. 972696.
[43] S. J. Chen et al., "A compact highly efficient and flexible polymer ultrawideband antenna," *IEEE Antennas Wireless Propag. Lett.*, vol. 14, pp. 1207–1210, 2015.
[44] R. Bancroft, "Microstrip antenna efficiency and surface wave loss," *IEEE Trans. Antennas Propag.*, vol. 69, no. 8, pp. 5032–5035, Aug. 2021.
[45] Q. H. Dang, S. J. Chen, and C. Fumeaux, "Thermographic investigation of frequency-reconfigurable wearable antennas," in *Proc. 16th Eur. Conf. Antennas Propag. (EuCAP)*, 2022, pp. 1–4.

PURNA B. SAMAL (Graduate Student Member, IEEE) received the B.E. degree in electrical engineering from the College of Science and Technology, Royal University of Bhutan (RUB), Bhutan, in 2008, and the M.E. degree in electrical engineering from Katholieke Universiteit Leuven (KU Leuven), Belgium, in 2013. He is currently pursuing the Ph.D. degree with the School of Electrical and Electronic Engineering, The University of Adelaide, Adelaide, SA, Australia.

From 2009 to 2019, he was a Lecturer with the Electronics and Communication Engineering Department, College of Science and Technology, RUB. During his tenure, he also served as a Programme Leader of Instrumentation and Control Engineering from 2018 to 2019, a member of the College Research Committee from 2015 to 2019, and the College Staff Secretary from 2015 to 2018. His current research interest includes wearable antenna design, flexible ultrawideband antennas, wireless body area network, unconventional conductive and dielectric materials for wearable antenna design, and drone application for rescue operation.

Mr. Samal was the recipient of the 2014–2015 Annual University Research Grant, Royal University of Bhutan. He received the 2011 EXPERTS (Exchange by Promoting Quality Education, Research and Training in South and South-East Asia) Scholarship and the 2019 Adelaide Scholarship International. He was awarded a Grant Funded Supplementary Scholarship from December 2019 to 2021. He has reviewed papers for *Microwave and Optical Technology Letters* and the *International Journal of RF and Microwave Computer-Aided Engineering*.

SHENGJIAN J. CHEN (Member, IEEE) received the M.E. and Ph.D. degrees in electrical and electronic engineering from The University of Adelaide, Australia, in 2013 and 2017, respectively.

From 2017 to 2021, he was a Postdoctoral Researcher and a Lecturer with the School of Electrical and Electronic Engineering, The University of Adelaide. He joined the College of Science and Engineering, Flinders University, Australia, as a Lecturer in 2022. He was a Top Reviewer for IEEE TRANSACTIONS ON ANTENNAS AND PROPAGATION in 2021. His current research interests include antenna design and engineering, wearable technology, microwave absorbers, and electromagnetic structures using advanced materials.

Dr. Chen received scholarships, including the Australian Postgraduate Award 2013 and the Simon Rockliff Scholarship 2015. He was also the recipient of several awards, including the Young Scientist Best Paper Award at the International Conference on Electromagnetics in Advanced Applications (ICEAA) 2015, the Young Scientist Best Paper Award and Travel Bursary Award at ICEAA 2016, an Honorable Mention at IEEE AP-S Symposium on Antennas and Propagation (APS/URSI) 2017, a CST University Publication Award 2017, and the Best Paper Award at IEEE Asia–Pacific Microwave Conference 2021. He was the Chair of the IEEE South Australia Joint Chapter on Microwave Theory and Techniques and Antennas and Propagation from 2019 to 2020.

TRAN T. TUNG received the Bachelor of Material Engineering and Master of Material Technology degrees from the Hanoi University of Science and Technology, Vietnam, in 2001 and 2005, respectively, and the Ph.D. degree from Korea University (KU), South Korea, in 2010.

From 2010 to 2015, he was a Postdoctoral Researcher with KU in 2011, the University of South Bretagne, France, from 2011 to 2013, and CNRS, Strasbourg University, France, from 2013–2014. In 2015, he joined the University of Adelaide as an Industry Grant-Funded Researcher and was promoted to a Senior Researcher and a Lecturer with the School of Chemical Engineering and Advanced Materials in 2019. He is a Productive Scientist with Extensive International Research Experience having more than 90 refereed publications mainly in high impact international journals. He is also the author of 6 book chapters, and 3 patents and has presented at more than 20 international conferences. These publications attracted more than 3100 citations (H-index of 35). His main research interests include advanced materials for sensors, coatings, and printing applications, especially exploring new applications of 2-D materials beyond graphene.

Dr. Tung was received a number of awards, including an Outstanding Reviewer, the Chair Conferences, and an Invited Scholar Researcher.

DUSAN LOSIC received the Chemistry degree from the Faculty of Natural Sciences and Mathematics, University of Novi Sad, Serbia, and the Ph.D. degree in nanoscience and nanotechnology from the School of Chemistry and Physical Science, Flinders University, Adelaide, SA, Australia, in 2003.

He is a Full Professor with the School of Chemical Engineering and Advanced Materials, University of Adelaide. He is also the Director of the Australian Research Council (ARC) Graphene Hub for Enabled Industry Transformation (40 researchers) and the Leader of Nano Research Group (20 researchers). He published over 470 research papers in world-leading journals and conference proceedings, including 3 books, 20 book chapters, +300 peer-reviewed journal papers, +80 peer-reviewed conference papers, +120 conference abstracts/presentations, and 9 patents. These papers attracted 15 journal covers and +14.000 citations with an H-index of 65. His supervision and mentoring include +150 researchers in total: +25 Visiting scientists/students, 18 Research Fellows, 30 Ph.D. (18 completed) +15 Masters, and +70 Honours students. His research focused on fundamental, engineering, and applied aspects across disciplines of nanotechnology, chemistry, materials science, biology, and medicine made outstanding contributions to the development and applications of new nanomaterials for addressing problems in medicine (localized drug delivery, implants, biosensing), environment (water and soil purification, protective coating, and fire protection), agriculture (nutrients delivery and pest control), energy (supercapacitors and batteries) and industry (additive manufacturing and composites).

Prof. Losic was awarded an ARC Research Fellow from 2007 to 2011 and an ARC Future Fellow from 2012 to 2017 very Prestigious Fellowship from ARC. He was awarded +50 competitive National and Industry research grants with a total of $20M.

CHRISTOPHE FUMEAUX (Fellow, IEEE) received the Diploma and Ph.D. degrees in physics from ETH Zürich, Switzerland, in 1992 and 1997, respectively.

From 1998 to 2000, he was a Postdoctoral Researcher with the School of Optics, University of Central Florida, Orlando. In 2000, he joined the Swiss Federal Office of Metrology, Bern, Switzerland, as a Scientific Staff Member. From 2001 to 2008, he was a Research Associate and a Lecturer with the Laboratory for Electromagnetic Fields and Microwave Electronics, ETH Zürich. Since 2008, he has been with The University of Adelaide, Australia, where he is currently a Professor with the School of Electrical and Electronic Engineering. His main research interests concern applied electromagnetics, antenna engineering, and the application of RF design principles across the electromagnetic spectrum.

Prof. Fumeaux was the recipient of the ETH Medal for his doctoral dissertation. From 2011 to 2015, he was a Future Fellow of the Australian Research Council. He received the 2018 Edward E. Altshuler Prize, the 2014 IEEE SENSORS JOURNAL and the 2004 ACES Journal Best Paper Awards, and the University of Adelaide Stephen Cole the Elder Award for Excellence in Higher Degree by Research Supervisory Practice in 2018. He also received the best conference paper awards at the 2012 Asia–Pacific International Symposium on Electromagnetic Compatibility and the 17th Colloque International sur la Compatibilité Electromagnétique 2014. More than ten of his students have received student awards with joint papers at IEEE conferences. He served as an Associate Editor for the IEEE TRANSACTIONS ON MICROWAVE THEORY AND TECHNIQUES from 2010 to 2013. From 2013 to 2016, he served as a Senior Associate Editor and later as the Associate Editor-in-Chief for the IEEE TRANSACTIONS ON ANTENNAS AND PROPAGATION. From 2017 to early 2023, he served as the Editor-in-Chief for the IEEE ANTENNAS AND WIRELESS PROPAGATION LETTERS.